# Photoinitiated Processes in Complexes: Subpicosecond Studies of $CO_2$—HI and Stereospecificity in Ar—HX

**C. Jaques, L. Valachovic, S. Ionov, E. Böhmer, Y. Wen, J. Segall† and C. Wittig***
*Department of Chemistry, University of Southern California, Los Angeles, CA 90089-0482, USA*

Build-up times for the OH product of photoinduced reactions in $CO_2$—HI complexes were measured for the photolysis wavelength range 235–263 nm by using the subpicosecond resolution pump–probe method pioneered by Zewail and co-workers. There is reasonable accord with theory and recent results from crossed-molecular-beams experiments. To illustrate the squeezed-atom effect, complementary measurements of hydrogen atom translational-energy distributions were carried out by using the high resolution high-*n* Rydberg time-of-flight (HRTOF) method of Welge and co-workers. Prototypical cases of Ar—HBr and Ar—HI complexes are reported. The former illustrates the squeezed-atom effect or caging of the exiting hydrogen. The latter is dominated by the formation of radical–molecule complexes. Extensions to other radical–molecule complexes are discussed.

Several aspects of reaction dynamics and inelastic scattering are discussed in this paper for experimental situations in which atomic hydrogen is the main energetic species in the entrance channel. In each case, photoinitiation of the desired event is carried out in a weakly bound complex that provides entrance channel constraint relative to the corresponding homogeneous gas-phase process. Our group has used three complementary approaches to investigate reactions in complexes: (i) Pump–probe experiments on a nanosecond time-scale yielded most of the initial information about reactions in complexes, such as product internal and translational excitations, as well as branching ratios for chemically distinct product channels. Comparisons between these results and information obtained from experiments under single-collision gas-phase conditions set the stage for (ii) time-domain femtochemistry studies[1] of reactions that are bimolecular for the most part, though strictly speaking the entrance channel environment provided by complexes is termolecular, and (iii) measuring hydrogen atom translational-energy distributions with high resolution by using the high-*n* Rydberg time-of-flight (HRTOF) technique.[2] The present paper focuses on the time-domain and HRTOF studies.

The femtochemistry studies reported here focus on two familiar reactions that involve photolytically prepared fast hydrogen atoms:

$$H + CO_2 \rightleftharpoons HOCO^{\dagger} \rightleftarrows CO + OH; \quad \Delta H = 8960\ cm^{-1} \quad (1)$$

$$H + N_2O \rightleftharpoons HNNO^{\dagger} \rightleftarrows OH + N_2; \quad \Delta H = -21\,820\ cm^{-1} \quad (2a)$$

$$\rightleftarrows NH + NO; \quad \Delta H = 12\,350\ cm^{-1} \quad (2b)$$

$$H + N_2O \rightarrow HONN \rightarrow OH + N_2; \quad \Delta H = -21\,820\ cm^{-1} \quad (2c)$$

where reaction (2*c*) proceeds by direct attack at the oxygen (*cf.* the two entrance channels in Fig. 2). Unlike reaction (2*a*), there is no long-lived intermediate in reaction (2*c*), HONN occupies a flat part of the potential-energy surface.[3,4] These two systems are shown schematically in Fig. 1 and 2.

Reaction (1) has received and continues to receive considerable attention, as it is deemed the second most important reaction in combustion, following $H + O_2 \rightleftharpoons OH + O$.[5,6] In just the past few years, several important aspects of reaction (1) have been reported. Zewail and co-workers pioneered the femtochemistry technique, in part by proving that bimolecular reactions were accessible to time-domain studies by using weakly bound complexes as precursors; $CO_2$—HI was their first example.[7,8] Following our discovery that $CO_2$—HBr and $CO_2$—HCl complexes have qualitatively different structures, *i.e.* end-on OCO—HCl and inertially T-shaped $CO_2$—HBr,[9,10] pump–probe studies on a nanosecond time-scale demonstrated the presence of a large steric effect in which broadside hydrogen attack at the oxygen was shown to be more favourable than end-on attack.[11] This is in accord with the known qualitative features of the potential-energy surface.[12] Smith and co-workers deduced the geometry of the H—OCO transition-state region by measuring nascent $CO_2$

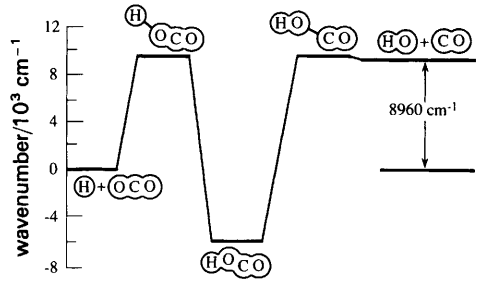


**Fig. 1** Reaction coordinate diagram for $H + CO_2 \rightleftharpoons HOCO \rightleftharpoons OH + CO$

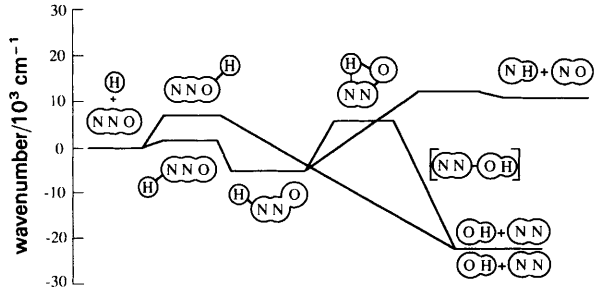


**Fig. 2** Reaction coordinate diagram for the $H + N_2O$ system. Pathways are depicted for O-atom attack, N-atom attack, and 1,3-hydrogen shift.

† Present address: Department of Chemistry, University of California, Irvine, CA 92717, USA.

vibrational-level populations and then making the assumption that all of the product vibrational excitation starts as bending potential energy at the transition state.[13] This inferred transition state differs considerably from the one predicted theoretically (*e.g.* an OCO angle of 171° *vs.* 159° theoretically[12]), thus providing grist for the mill of theory. Several theoretical treatments of this system that calculate reaction rates and product-state distributions, ranging from quasiclassical trajectories[14] to quantum scattering calculations,[15] are now converging and are in agreement with RRKM predictions[16] that used experimentally derived parameters.

In the present paper, we report OH build-up times for $CO_2$—HI complexes that are photoexcited in the wavelength range 235–263 nm. The results agree with theory as well as can be expected, considering the uncertainties present in both the theories and the experiments. Though the present rates are faster than those reported by Scherer *et al.*,[8] the experimental differences are enough to make a one-to-one comparison difficult; this will be discussed in a future publication.[17] If the 1990s indeed become the decade that takes us beyond A + BC, reaction (1) may prove to be an important prototype, even more so than OH + $H_2$ with its three hydrogens.

Reaction (2) has been shown to yield OH + $N_2$ *via* the HNNO intermediate, which accesses the exit channel by transferring the hydrogen atom to the oxygen side. This 1,3-hydrogen shift mechanism was first suggested by Marshall and co-workers,[3] who studied reaction (2) in the temperature range 390–1310 K. Böhmer *et al.* showed that it was the dominant mechanism in fast hydrogen atom reactions also.[18] However, product-state distributions obtained for the reaction in complexes do not allow one to draw unambiguous conclusions about how the reaction proceeds in this environment.

Stereochemically, reaction (2) is well suited for experiments that exploit $N_2O$—HI precursors and real-time monitoring of product build-up. *Ab initio* calculations[19] suggest that hydrogen spends more time near the oxygen than near the terminal nitrogen; the central nitrogen is not favourable at all. However, one must bear in mind that in such complexes hydrogen has a very large zero-point amplitude. Reaction (2) raises interesting issues. For example, will photoinitiated reactions in complexes influence the OH production mechanism, *i.e.* reaction (2*a*) *vs.* (2*c*)? Alternatively, will the entrance channel environment prove to be important by enabling iodine to bond to the departing OH or to the terminal nitrogen in HNNO, or will iodine bond to form transitory INH or INO species? Several of these questions can be answered by the use of time-domain studies. For example, reaction (2*c*) will produce OH more rapidly than reaction (2*a*). Initial results for this system are presented below. The data show a characteristic OH build-up time of less than 300 fs from $N_2O$—HI complexes excited at 250 nm. Signal amplitudes are quite reasonable and technical changes in our apparatus will soon give < 100 fs resolution.

For chemical systems such as those depicted in eqn. (1) and (2), state-resolved and time-domain probing of product species helps us to unravel the dynamics of reactions involving fast hydrogen atoms. However, both methods are blind to the majority of the hydrogen atoms, which simply undergo inelastic scattering. The question then remains: what happens to hydrogen atoms that do not react? It makes sense to address this issue initially by using a simple system for which a thorough theoretical treatment is possible.

Consequently, in a series of complementary studies, the HRTOF method was used to examine hydrogen atoms that scatter inelastically from complexes of the form Rg—HX, where Rg is a rare-gas atom. If the Rg—HX ground-state equilibrium structure favours hydrogen residing between Rg and X, photodissociation of the HX moiety will cause at least some of the hydrogen to rebound from Rg as it exits. In addition, hydrogen transmits forces to the heavier objects, and therefore its final speed is 'red shifted' relative to that of uncomplexed HX. This has been termed the squeezed-atom effect[20] and caging[21] in earlier papers. Results for Ar–HBr presented below demonstrate this effect clearly. Alternatively, if the hydrogen in Rg—HX is highly delocalized or prefers to point away from Rg, little or no red-shift is anticipated. In fact, if Rg—X is more strongly bound than Rg—HX, the hydrogen can be 'blue-shifted'. This effect is observed for Ar—HI, where Ar—I complexes are produced by the photolytic removal of atomic hydrogen. The distribution of HI axes relative to the new Ar—I quantisation axis determines how the I($^2P_J$) orbitals project onto the Ar—I axis. This draws upon earlier work by Aquilanti and co-workers.[22] Results with HI—HBr complexes indicate the formation of I—HBr, another attractive species, and other photodissociation results support the premise that the rapid photolytic removal of atomic hydrogen is a generally favourable means of preparing radical–molecule complexes.

## Experimental

### Subpicosecond Resolution Pump–Probe Studies

The apparatus is similar to that used previously,[23] so only details germane to the current study are presented, see Fig. 3. Measurements are carried out in a vacuum chamber equipped with a pulsed expansion source (250 μs duration, 0.25 mm × 1 mm aperture), a quadrupole mass spectrometer, and a photomultiplier tube (PMT) and collection optics for laser induced fluorescence (LIF) measurements. Complexes are formed by expanding mixtures of 2% HI, 3% $CO_2$ and

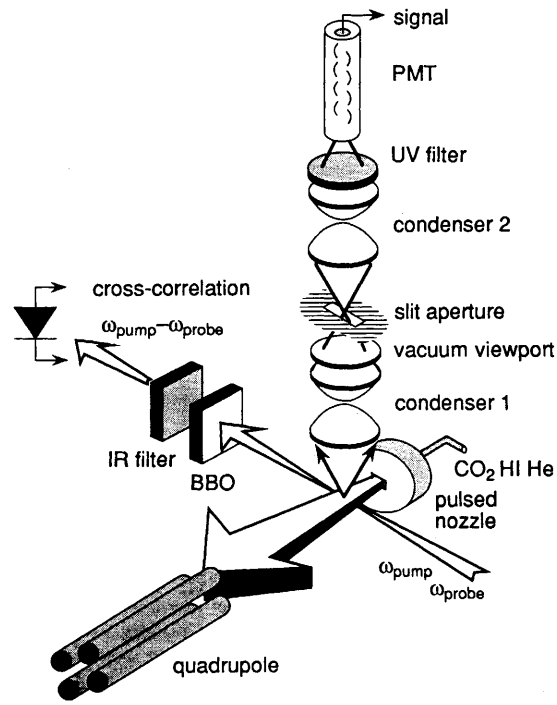


**Fig. 3** Schematic representation of the experimental technique used to measure OH build-up rates. Complexes are formed by expanding gas mixtures supersonically from a piezoelectric pulsed nozzle. OH products are detected by using LIF. Co-propagating pump and probe beams are mixed in a BBO crystal to obtain the difference frequency for the cross-correlation measurements.

95% He through the nozzle at a stagnation pressure of 2.3 atm†. Mixtures are kept in a stainless steel cylinder and before entering the nozzle they are passed through a cold trap at −90 °C which removes $I_2$ without freezing $CO_2$ and HI. The nozzle effluent is monitored by the mass spectrometer, which is located across the chamber from the pulsed nozzle. Signals from $(CO_2)_2HI^+$ and $CO_2(HI)_2^+$ were less than 15% of that from $CO_2HI^+$.

Reactions are initiated and probed with subpicosecond laser pulses. The primary source of tunable subpicosecond radiation is a dual-jet dye laser which is synchronously pumped by the second harmonic of an actively mode-locked Nd : YAG laser. Typically, 1.8 W is obtained at 532 nm after frequency doubling in LBO. The dye laser output is a 76 MHz train of 500 fs pulses at 618.2 nm. Dye laser pulses are sent through a three-stage dye amplifier which is pumped by the second harmonic of a 10 Hz regenerative amplifier (RGA). Normally, 35 mJ (532 nm) and 45 mJ (355 nm) pulses of *ca.* 70 ps duration are obtained by doubling and tripling the RGA output. The dye amplifier yields 1 mJ pulses at 618.2 nm and this is divided into two beams. The first, containing *ca.* 80% of the energy, is doubled in KDP, producing 40–100 μJ, 500 fs pulses at 309.1 nm; the bandwidth of *ca.* 80 $cm^{-1}$ is at least four times broader than the Fourier transform limit. The 309.1 nm pulses are used to probe OH *via* $A\,^2\Sigma \leftarrow X\,^2\Pi$ LIF. The spectral width of the probe is broad enough to excite OH rotational states from $N = 2$ to 20 with $\langle N \rangle \approx 5.5$.

The remaining 20% of the amplified 618.2 nm pulse is focused with a 10 cm focal length lens into a $D_2O$ cell producing a continuum. This light is recollimated and vertical polarisation is selected. A desired wavelength between 470 and 526 nm is filtered from the continuum with a double-pass grating monochromator;[9,24] no temporal broadening of spectrally selected pulses is observed for slit openings larger than 0.6 mm. The spectrally selected pulses are amplified in a two-stage dye amplifier pumped by the RGA third harmonic. Depending on the wavelength, the amplifier delivers 0.3–1.5 mJ pulses with no significant temporal broadening. The amplified beam is doubled in BBO and the resulting pulses are used to photodissociate HI and thus trigger chemical transformations leading to OH production. Pump bandwidths of 80 $cm^{-1}$ are close to that of the probe.

After passing through a computer-controlled delay stage the probe and pump beams are combined on a dichroic mirror and focused onto the supersonic jet *ca.* 5 mm downstream from the nozzle. Since the pump and probe beams have different divergences, independent focusing is required to optimise their spatial overlap in the focal plane. Typical LIF signals do not exceed a few photons per laser shot. Thus, precautions are needed to reduce the amount of scattered laser light reaching the PMT: entrance and exit windows are mounted at the Brewster angle on long arms 55 cm from the jet axis; a set of baffles is positioned inside the arms; a filter with 250–390 nm transmission is put in front of the PMT to block scattered pump radiation; and LIF is spatially filtered by a 5 mm × 25 mm slit in the focal plane of the first condenser. Fluorescence that passes through the slit is focused onto the PMT.

Signals are amplified, digitized and collected in a computer which counts photons appearing between 70 and 1200 ns after the laser pulses. Simultaneously with the LIF, a pump–probe cross-correlation signal is recorded. This is obtained by focusing both pump and probe beams into a 100 μm BBO crystal and generating a difference frequency. This radiation is focused onto a Ge photodiode. For the longest pump wavelength, 263 nm, the difference frequency, 1760 nm, falls near the long wavelength cut-off of the detector, and consequently the cross-correlation signal is very weak. For this pump wavelength the cross correlation is obtained from transient measurements of OH produced from UV photolysis of hydrogen peroxide, as discussed below.

### High-*n* Rydberg Time-of-flight

A full description of the experimental method of high resolution high-*n* Rydberg time-of-flight (HRTOF) spectroscopy is not possible here; details are published elsewhere.[2,25] Fig. 4(*a*) shows the salient features: (i) expansion cooling of samples using a pulsed nozzle; (ii) 193 and 248 nm excimer laser photodissociation; (iii) Lyman-α excitation of atomic hydrogen with sub-Doppler resolution; (iv) further excitation of the excited hydrogen to optically metastable high-*n* Rydberg states lying just below the ionisation continuum; and (v) ionisation of the high-*n* hydrogen atoms as they pass a mesh in front of the microchannel plate, thereby providing the TOF spectrum. Fig. 4(*b*) shows a spectrum obtained by varying the wavelength of the Rydberg excitation step while monitoring the microchannel-plate signal. In addition to the desired binary complexes, there are undoubtedly higher-than-binary complexes present under the present experimental conditions. These must be taken into consideration when analysing the data.

Polarised photolysis radiation enables the transition dipoles of dissociating molecules to be aligned. For hydrogen halides, parallel and perpendicular transitions show strong halogen atom spin–orbit preferences, as has been observed when photolysing uncomplexed material.[26] This can be used

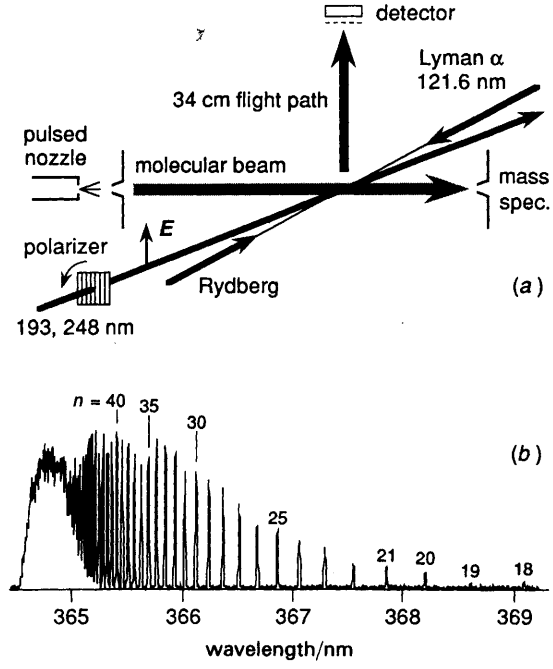


**Fig. 4** Schematic representation of the experimental technique used for high resolution high-*n* Rydberg time-of-flight (HRTOF) measurements of hydrogen atoms. Samples are expansion cooled through a pulsed nozzle and photodissociated at 193 and/or 248 nm. Atomic hydrogen is first excited at Lyman-α with sub-Doppler resolution and further excited to optically metastable high-*n* Rydberg states. TOF spectra of the highly excited hydrogen atoms are obtained by removing the weakly bound electrons as the excited hydrogen atoms pass a wire mesh. The resulting protons are detected at a microchannel plate.

† 1 atm = 101 325 Pa.

to advantage in inelastic scattering studies with complexes. Specifically, it is possible to set the laser polarisation such that a minimal number of hydrogen atoms reach the detector following HX photolysis, *i.e.* they move mostly perpendicular to the line from the photolysis region to the detector. Under these conditions, scattering of hydrogen from the nearby moiety can result in large signal enhancements, *i.e.* when the hydrogen atom would miss the detector unless it scatters from the nearby species.

A typical HRTOF spectrum is shown in Fig. 5 for the case of 248 nm HI photodissociation; signal averaging for *ca.* 15 min results in a signal to noise ratio (*S/N*) of *ca.* 3000. The two iodine spin–orbit states are separated by 7603 $cm^{-1}$. Because of the high *S/N* and resolution, it is possible to observe inelastic scattering on the low-energy side of the peaks, as shown below.

## Results and Discussion

Results for $CO_2$—HI photolysis in the wavelength rage 235–263 nm are presented in Fig. 6. The OH build-up times ranged from 250 to 1500 fs, respectively, (*vide infra*) and the pump–probe cross correlations were measured simultaneously with the LIF signals. Scans were taken over periods of 1–4 h depending on the signal intensities. Maximum signals of *ca.* 2 photons per laser firing were obtained at $\lambda_{pump}$ = 240 nm; this decreased to *ca.* 0.3 photons per laser firing at $\lambda_{pump}$ = 263 nm. This decrease of signal with increasing excitation wavelength derives from drops in both the HI absorption coefficient and the cross-section for reaction (1). It has not yet been possible to measure rates closer to threshold.

Several checks were made to ensure that the LIF signals derived predominantly from OH generated *via* the photoexcitation of $CO_2$—HI. First, the probe was detuned from 309.1 nm to 304 nm and the LIF signal disappeared completely, as expected. When either $CO_2$ or HI was removed from the sample, no transient signal whatsoever was observed for $\lambda_{pump}$ < 255 nm. However, at 260 nm, a sharp temporal peak was detected for HI–He samples, which had the same shape as both the cross correlation and the peak superimposed on the 260 nm $CO_2$—HI scans, as shown in Fig. 6. These features were also observed with HI–He samples for $\lambda_{pump}$ = 263 and 255 nm but at much lower intensities. Since the simultaneous presence of the pump and probe is required for this signal to be observed, it is attributed tentatively to two-colour, two-photon absorption to high HI electronic states. The intensity of such a process is proportional to the temporal overlap between the beams so the peak shape is described by the pump–probe cross correlation. In data analyses, a weighted cross-correlation signal was subtracted from the transient LIF signal for $\lambda_{pump}$ = 260 nm and no correction was made for any other wavelengths.

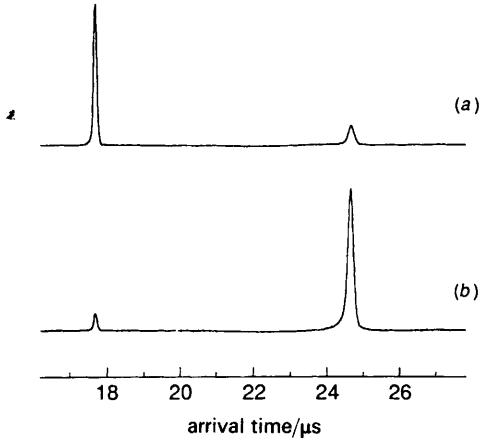


**Fig. 5** HRTOF spectra for 248 nm photodissociation of HI. (*a*) Horizontal polarization, (*b*) vertical polarization. The peaks for $I(^2P_{3/2})$ and $I(^2P_{1/2})$ derive mainly from perpendicular and parallel transitions, respectively. Experimental resolution is *ca.* 70 $cm^{-1}$, *i.e.* the excimer laser linewidth; *S/N* is *ca.* 3000.

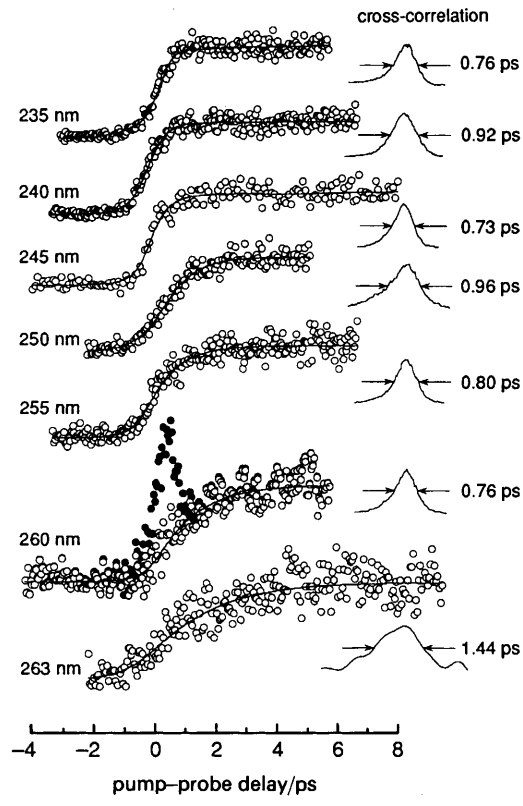


**Fig. 6** Representative traces of OH LIF signal *vs.* pump–probe delay from the photoinitiated reaction: $CO_2$—HI + $h\nu \rightarrow$ HOCO$^\dagger$ + I → OH + CO + I. The number of photon counts is plotted *vs.* pump–probe delay for various pump wavelengths. The solid line is the least-squares fit to the data; see text for details. The corresponding pump–probe cross-correlation, obtained by difference frequency generation in BBO, is also shown. The black data points for the 260 nm trace are due to two-colour, two-photon LIF of HI.

An outstanding problem in such experiments is quantifying the role of higher-than-binary complexes.[27] As stated above, for the present experimental conditions, the $(CO_2)_2HI^+$ and $CO_2(HI)_2^+$ signals were less than 15% of the $CO_2HI^+$ signal. However, the mass spectrometer cracking patterns of $(CO_2)_m(HI)_n$ complexes are not known, so this is only suggestive that binary complexes dominate. Changing the amount of $CO_2$ in the sample allowed cluster concentrations to be varied, and a linear decrease in the OH LIF signal was observed as the $CO_2HI^+$ signal was lowered. At the other extreme, when increasing the HI concentration to 10%, the amount of higher clusters increased and the OH LIF signal intensity decreased. Interestingly, the time dependence did not change. Thus we conclude that though higher-than-binary complexes are present under our experimental conditions, the results reflect mainly binary complexes.

For the case of $N_2O$—HI, the OH LIF signal intensity *vs.* pump–probe delay is presented in Fig. 7. At $\lambda_{pump}$ = 250 nm the build-up time is < 300 fs, *i.e.* not resolvable at the present experimental resolution. Since signal intensities are high (*ca.* 5 photons per laser shot) this experiment will be continued when pulse compression is implemented, yielding temporal

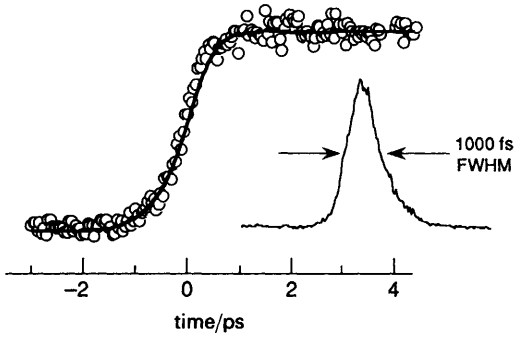


**Fig. 7** Representative experimental scan and corresponding cross-correlation for the reaction $N_2O$—HI + $h\nu \rightarrow$ OH + $N_2$ + I. HI was photolysed at 250 nm plotted *vs.* the delay between the pump and probe pulses. The solid line is the fit to the data using eqn. (3) and (4). The OH build-up time is less than 300 fs.

resolution $<100$ fs. Referring to Fig. 2, the HNNO intermediate is expected to be short lived because it can decompose easily to H + $N_2O$. Though the HNNO$^\dagger$ lifetime can be less than 300 fs, we anticipate that resolution of $<100$ fs will allow us to decide definitively between reaction (2*a*) and (2*c*).

Data were fit by using the following equations with a non-linear least-squares fitting routine:

$$S(t) \propto \int_{-\infty}^{t} R(s)\{1 - \exp[-(t-s)/\tau]\}\, ds \qquad (3)$$

$$R(s) = \int_{-\infty}^{+\infty} I_{\text{pump}}(s+t) I_{\text{probe}}(t)\, d_t \qquad (4)$$

where $R(s)$ is the cross correlation. $S(t)$ is the signal as a function of pump–probe delay time, and $[1 - \exp(-t/\tau)]$ is the assumed form of the molecular-response function. These equations implicitly assume that coherence effects are not important. One justification of this assumption is the broad bandwidth of the laser pulses, several times the Fourier-transform limit. Another is the unimolecular process itself: phases of the OH fragments are poorly correlated because of the chaotic dynamics of HOCO$^\dagger$ decomposition.

As an experimental check, eqn. (3) and (4) were used to fit the time-resolved photodissociation of hydrogen peroxide. This is a direct process and thus products can evolve coherently. With our temporal resolution, the rise-time was essentially instantaneous and there were no recurrences or undulations at long times. In another check, the laser pulses were temporally broadened to 1.2 ps and narrowed spectrally to 30 cm$^{-1}$. These pulses yielded the same reaction rates as did the shorter pulses.

Fig. 8 presents the OH build-up rates that are obtained at different excitation wavelengths when fitting the data by using eqn. (3) and (4). The horizontal axis is the HOCO$^\dagger$ energy in excess of reaction threshold, $E^\dagger$. Obviously, there is latitude in assigning $E^\dagger$ values to the measured rates because of the uncertainty in the I—HOCO translational recoil energy. The maximum possible $E^\dagger$ values (*i.e.* the upper bounds) are for the corresponding single-collision gas-phase conditions in which there are no three-body effects in the entrance channel. Open circles represent this case. To estimate the possible magnitude of the squeezed atom effect, namely, to what extent $E^\dagger$ is lowered by the three-body entrance channel environment, we refer to our earlier studies of OH rotational distributions. In comparing the measured OH rotational distributions obtained with complexes to those obtained under single-collision gas-phase conditions,[20] we found that most of the data could be reconciled by lowering the H + $CO_2$ 'collision energy' in complexes by *ca.* 10%.

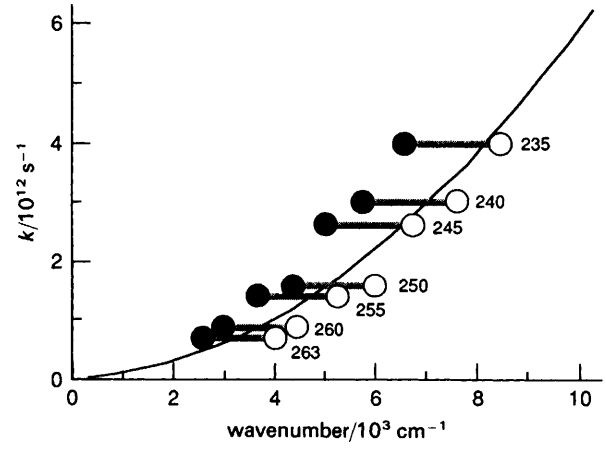


**Fig. 8** Reaction rates for the indicated photolysis wavelengths. The open circles represent the $E^\dagger$ values that would be associated with the corresponding single-collision gas-phase conditions, *i.e.* photolysis of uncomplexed HI followed by H + $CO_2$ collisions. This is an upper limit to $E^\dagger$. The closed circles represent $E^\dagger$ values that are lower than the corresponding gas-phase values due to the squeezed-atom effect.

Filled circles in Fig. 8 represent this 10% decrease in collision energy. The horizontal bars connecting the open and filled circles are for visual convenience. What we concluded is that for each excitation wavelength there is a range of $E^\dagger$ values whose average is near the filled circle. As shown below, photodissociation of the HBr in Ar—HBr complexes reveals a decrease of hydrogen translational energies; a direct confirmation of the squeezed atom effect.

The solid curve in Fig. 8 is an earlier RRKM estimate.[16] The trajectory calculations of Schatz and co-workers[14] (not shown) are close to the filled circles. Agreement with the quantum-scattering calculations of Clary and co-workers[15] is also good. In addition, the recent OH + CO crossed-molecular-beams experiments of Casavecchia and co-workers[28] yield HOCO$^\dagger$ lifetimes that are in accord with our experiments. It appears that, within the admittedly significant uncertainties, some convergence is at hand for the rate constant, though other important questions remain.

One of the main scientific implications of the results of the present rate measurements is that, for whatever reason, transition-state theory retains its predictive capacity at high energies. At 235 nm, $E^\dagger$ is *ca.* 8000 cm$^{-1}$, while the HOCO well-depth is only *ca.* 14 000 cm$^{-1}$. Also, OH build-up times of 250 fs are short enough to question the underlying assumption of fast intramolecular vibrational redistribution (IVR). Nevertheless, RRKM predictions give good results. Hopefully, more rigorous theories will explain why this is so.

Next, we turn to the fast hydrogen atoms that are prepared photolytically in complexes but do not go on to react. Though our measurements are not, in principle, limited to processes involving atomic hydrogen, it turns out that all the experiments reported here have involved atomic hydrogen in one way or another. This leads naturally to applications of the HRTOF method described in the Experimental section. The results obtained by using the HRTOF method complement the subpicosecond resolution studies. For example, with photoexcited complexes the squeezed-atom effect involving atomic hydrogen has been invoked to explain both nascent product-state distributions[20] and unimolecular rate constants, but this effect had not previously been observed directly. To observe this effect experimentally, we used complexes of the form Rg—HX. Inelastic scattering in such complexes had been predicted by Gerber and co-workers,[21] who showed that low-energy tails in the hydrogen kinetic energy distributions are characteristic of the squeezed-atom effect in

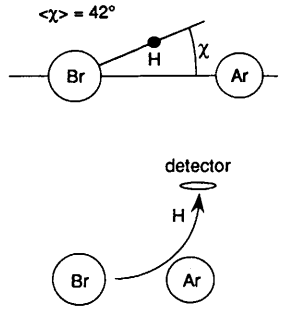


**Fig. 9** Schematic drawing showing the Ar—HBr structure and a hypothetical situation in which a hydrogen atom that would otherwise miss the detector is scattered toward the detector by the nearby Ar.

complexes such as Ar—HBr where the hydrogen resides primarily between the heavier atoms, as shown in Fig. 9. Structural properties of the Ar—HBr complex were determined accurately by Flygare and co-workers by using high-resolution spectroscopy.[29] Note the very large zero-point amplitude, which suggests that bonding is due to both the weakly acidic hydrogen and the dispersive Ar—Br interaction. An experimental verification of the squeezed-atom effect is shown in Fig. 10. The HBr transition moment is primarily perpendicular, so the horizontally polarised laser gives larger signals, by a factor of *ca.* 6, than the vertically polarised laser. Though not shown, agreement with theory is very good.[30]

The case of vertical laser polarisation displays an interesting feature that we plan to examine further. The lower entry in Fig. 9 depicts a situation in which the hydrogen atom would have missed the detector had it not scattered from the nearby Ar. This would be the case for a purely perpendicular transition and vertical laser polarisation: only hydrogen atoms that are strongly scattered can reach the detector. This effect is shown in the upper trace of Fig. 10(*c*), though there is a contribution from a parallel transition, particularly in the Br($^2P_{1/2}$) channel, that we hope can be eliminated in the future by a judicious choice of photolysis wavelength. Nevertheless, we can see in Fig. 10(*c*) that signals deriving from uncomplexed HBr (as well as from hydrogen atoms that are only weakly scattered) are low relative to those deriving from hydrogen atoms that are strongly scattered. These appear as two broad features, shifted *ca.* 1000 $cm^{-1}$ to the red of the unscattered peaks. This indicates that hydrogen atoms which interact strongly with their heavy neighbours have 5–10% less energy than those from uncomplexed HBr. By analysing the full angular dependence, it may be possible to deconvolute the scattering tha occurs within the Ar—HBr frame.

Finally, we would like to discuss cases in which the hydrogen atom leaves without recoiling from anything except the iodine. To examine this experimentally, Ar–HI mixtures were expanded, thereby forming complexes. At this preliminary stage, little can be said about the role of higher-than-binary complexes. In the complexes formed, we believe that the non-acidic hydrogen has little reason to be found preferentially between Ar and I; rather, the dispersive Ar—I attraction is expected to dominate. The resulting HRTOF spectra differ qualitatively from those obtained with Ar–HBr mixtures. As shown in Fig. 11, there is very little red shift. Instead of the predominant red shifts seen with Ar—HBr, there is actually a prominent blue shift, *i.e.* tail toward higher energies. What this proves is that Ar—I (or $Ar_n$—I) remains bound, since having free species such as H + I + Ar requires both the H—I and Ar—HI bonds to be broken, which would cause a red shift.

There are two primary sources of 'additional' hydrogen translational energy, *i.e.* in excess of that from HI photodissociation. One is trivial: hydrogen shares $E_{CM}$ with whatever photoproduct remains, and the energy partitioning depends on the mass ratio due to momentum conservation. Therefore the hydrogen atom gets a larger share of $E_{CM}$ when the photoproduct is $Ar_n$—I than when it is just I. However, the gain in translational energy due to this mechanism is only 30 $cm^{-1}$ for Ar—HI and cannot possibly exceed 15700/127 = 124 $cm^{-1}$ (for $Ar_n$—HI with large *n*). The tail shown in Fig. 11 extends well past this. Secondly, if the Ar—I bond is stronger than the Ar—HI bond, the departing hydrogen can take up some or all of this increase in the binding energy. We suspect this to be the case. In any event, there is no red shift to speak of, so the result of photolysis is to leave behind a radical–molecule complex.

These radical–molecule complexes have been widely sought after: witness the work of the groups of Lester,[31] Heaven,[32] Miller,[33] and Neumark,[34] and the excitement their results have brought to the field. We suggest that the present method is viable for a broad range of systems and that high concentrations (*ca.* $10^{14}$ $cm^{-3}$) can be prepared, making high-resolution spectroscopic studies practical. Moreover, many of these complexes are of a practical nature for studying properties and reactivities of chemically interesting systems, and we predict that complexes of $CH_3O$, $CH_3S$ *etc.* with alkenes and alkynes will be prepared by using this method.

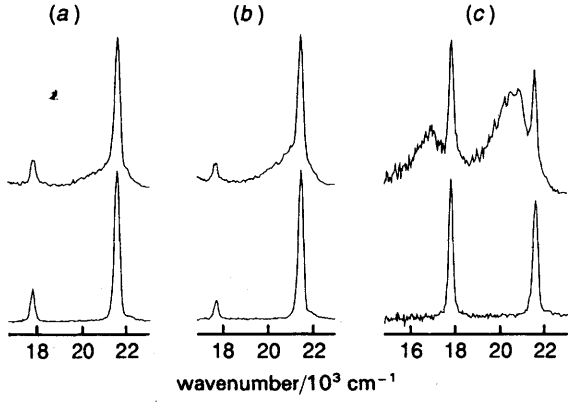


**Fig. 10** Experimental HR TOF data for Ar—HBr, transformed to yield kinetic energy distributions. The upper and lower traces correspond to significant and minimal clustering, respectively. (*a*) unpolarised; (*b*) horizontal polarisation and (*c*) vertical polarisation.

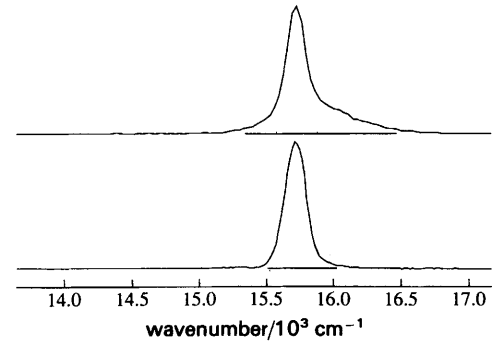


**Fig. 11** Representative HRTOF spectrum of expanded HI–Ar mixtures at 200 kPa backing pressure. The narrower feature is for minimal clustering. Note that hydrogen emerging from this environment has very little red shift and exhibits a significant high-energy tail (blue shift).

The authors have benefitted greatly from ongoing collaborations and interactions with R. A. Beaudet, H. Reisler and R. B. Gerber. This research was supported by the U.S. National Science Foundation and the U.S. Department of Energy.

## References


1 A. H. Zewail, *Faraday Discuss. Chem. Soc.*, 1991, **91**, 207.
2 (*a*) M. N. R. Ashfold, I. R. Lambert, D. H. Mordaunt, G. P. Morley and C. M. Western, *J. Phys. Chem.*, 1992, **96**, 2938; (*b*) L. Schneider, W. Meier, K. H. Welge, M. N. R. Ashfold and C. M. Western, *J. Chem. Phys.*, 1990, **92**, 7027.
3 (*a*) P. Marshall, T. Ko and A. Fontijn, *J. Phys. Chem.*, 1989, **93**, 1922; (*b*) P. Marshall, A. Fontijn and C. F. Melius, *J. Chem. Phys.*, 1987, **86**, 5540.
4 S. P. Walch, *J. Chem. Phys.*, 1993, **98**, 1170.
5 D. L. Baulch and I. M. Campbell, *Gas Kinetics and Energy Transfer*, Specialist Periodical Report, Royal Society of Chemistry, 1981, vol. 4, pp. 137–188.
6 G. W. Flynn, *Science*, 1989, **246**, 1009.
7 N. F. Scherer, L. R. Khundkar, R. B. Bernstein and A. H. Zewail, *J. Chem. Phys.*, 1987, **87**, 1451.
8 N. F. Scherer, C. Sipes, R. B. Bernstein and A. H. Zewail, *J. Chem. Phys.*, 1990, **92**, 5239.
9 S. W. Sharpe, Y. P. Zeng, C. Wittig and R. A. Beaudet, *J. Chem. Phys.*, 1990, **92**, 943.
10 Y. P. Zeng, S. W. Sharpe, S. K. Shin, C. Wittig and R. A. Beaudet, *J. Chem. Phys.*, 1992, **97**, 5392.
11 S. K. Shin, Y. Chen, D. Oh and C. Wittig, *Philos. Trans. R. Soc. A*, 1990, **332**, 361.
12 G. C. Schatz, M. S. Fitzcharles and L. B. Harding, *Faraday Discuss. Chem. Soc.*, 1987, **84**, 359.
13 M. J. Frost, J. S. Salh and I. W. M. Smith, *J. Chem. Soc., Faraday Trans.*, 1991, **87**, 1037.
14 K. Kudla and G. C. Schatz, *J. Chem. Phys.*, 1991, **95**, 1635.
15 D. C. Clary, *NATO Adv. Res. Workshop on Orientation and Polarization Effects in Chemical Reaction Dynamics, Perugia, Italy, 1992*, Paper 36.
16 G. Hoffmann, D. Oh, Y. Chen, Y. M. Engel and C. Wittig, *Israel J. Chem.*, 1990, **30**, 115.
17 C. Wittig and A. H. Zewail, unpublished.
18 E. Böhmer, S. K. Shin, Y. Chen and C. Wittig, *J. Chem. Phys.*, 1992, **97**, 2536.
19 Y. P. Zeng, S. Sharpe, D. Reifschneider, C. Wittig and R. A. Beaudet, *J. Chem. Phys.*, 1990, **93**, 183.
20 C. Wittig, Y. M. Engel and R. D. Levine, *Chem. Phys. Lett.*, 1988, **153**, 411.
21 (*a*) R. Alimi and R. B. Gerber, *Phys. Res. Lett.*, 1990, **64**, 1453; (*b*) A. García-Vela, R. B. Gerber and J. J. Valentini, *Chem. Phys. Lett.*, 1991, **186**, 223; (*c*) A. García-Vela, R. B. Gerber and J. J. Valentini, *J. Chem. Phys.*, 1992, **97**, 3297.
22 V. Aquilanti, G. Liuti, F. Pirani and F. Vecchiocattivi, *J. Chem. Soc., Faraday Trans. 2*, 1989, **85**, 955 and references therein.
23 G. A. Brucker, S. I. Ionov, Y. Chen and C. Wittig, *Chem. Phys. Lett.*, 1992, **194**, 301.
24 O. E. Martinez, *IEEE J. Quant. Electron.*, 1987, **23**, 59.
25 J. Segall, Y. Wen, R. Lavi, R. Singer and C. Wittig, *J. Phys. Chem.*, 1991, **95**, 8078.
26 Z. Xu, B. Koplitz and C. Wittig, *J. Chem. Phys.*, 1988, **92**, 5518.
27 S. K. Shin, Y. Chen, S. Nickolaisen, S. W. Sharpe, R. A Beaudet and C. Wittig, *Advances in Photochemistry*, ed. D. Volman, G. Hammond and D. Neckers, Wiley, 1991, vol. 16, pp. 249–363.
28 M. Alagia, N. Balucani, P. Casavecchia and G. G. Volpi, *NATO Adv. Res. Workshop on Orientation and Polarization Effects in Chemical Reaction Dynamics, Perugia, Italy, 1992*, Paper 18.
29 M. R. Keenan, E. J. Campbell, T. J. Balle, L. W. Buxton, T. K. Minton, P. D. Soper and W. H. Flygare, *J. Chem. Phys.*, 1980, **72**, 3070.
30 A. Garcia-Vela, R. B. Gerber, J. Segall, Y. Wen, R. Singer and C. Wittig, *Chem. Phys. Lett.*, submitted.
31 (*a*) M. T. Berry, M. R. Brustein and M. I. Lester, *J. Chem. Phys.*, 1990, **92**, 6469; (*b*) W. H. Green Jr. and M. I. Lester, *J. Chem. Phys.*, 1992, **96**, 2573.
32 (*a*) W. M. Fawzy and M. C. Heaven, *J. Chem. Phys.*, 1988, **89**, 7030; (*b*) W. M. Fawzy and M. C. Heaven, *J. Chem. Phys.*, 1990, **92**, 909.
33 L. Yu, J. Williamson, S. C. Foster and T. A. Miller, *J. Chem. Phys.*, 1992, **97**, 5273.
34 Y. Zhao, C. C. Arnold and D. M. Neumark, *J. Chem. Soc., Faraday Trans.*, 1993, **89**, 1449.


*Paper* 2/06860E; *Received 24th December*, 1992